AMERICAN SOCIETY FOR MICROBIOLOGY | Journal of Virology®

VIRUS-CELL INTERACTIONS

Porcine Deltacoronavirus Enters Porcine IPI-2I Intestinal Epithelial Cells via Macropinocytosis and Clathrin-Mediated Endocytosis Dependent on pH and Dynamin

Puxian Fang,[a,b] Jiansong Zhang,[a,b] Huichang Zhang,[a,b] Sijin Xia,[a,b] Jie Ren,[a,b] Liyuan Tian,[a,b] Dongcheng Bai,[a,b] Liurong Fang,[a,b] Shaobo Xiao[a,b]

[a]State Key Laboratory of Agricultural Microbiology, College of Veterinary Medicine, Huazhong Agricultural University, Wuhan, China
[b]Key Laboratory of Preventive Veterinary Medicine in Hubei Province, the Cooperative Innovation Center for Sustainable Pig Production, Wuhan, China

Puxian Fang and Jiansong Zhang contributed equally to this work. Author order was determined in order of increasing seniority.

ABSTRACT Porcine deltacoronavirus (PDCoV), an emerging enteropathogenic coronavirus, causes serious diarrhea in suckling piglets and has the potential for cross-species transmission. Although extensive studies have been reported on the biology and pathogenesis of PDCoV, the mechanisms by which PDCoV enters cells are not well characterized. In this study, we investigated how PDCoV enters IPI-2I cells, a line of porcine intestinal epithelial cells derived from pig ileum. Immunofluorescence assays, small interfering RNA (siRNA) interference, specific pharmacological inhibitors, and dominant negative mutation results revealed that PDCoV entry into IPI-2I cells depended on clathrin, dynamin, and a low-pH environment but was independent of caveolae. Specific inhibition of phosphatidylinositol 3-kinase (PI3K) and the Na^+/H^+ exchanger (NHE) revealed that PDCoV entry involves macropinocytosis and depends on NHE rather than on PI3K. Additionally, Rab5 and Rab7, but not Rab11, regulated PDCoV endocytosis. This is the first study to demonstrate that PDCoV uses clathrin-mediated endocytosis and macropinocytosis as alternative endocytic pathways to enter porcine intestinal epithelial cells. We also discussed the entry pathways of PDCoV into other porcine cell lines. Our findings reveal the entry mechanisms of PDCoV and provide new insight into the PDCoV life cycle.

IMPORTANCE An emerging enteropathogenic coronavirus, PDCoV, has the potential for cross-species transmission, attracting extensive attenuation. Characterizing the detailed process of PDCoV entry into cells will deepen our understanding of the viral infection and pathogenesis and provide clues for therapeutic intervention against PDCoV. With the objective, we used complementary approaches to dissect the process in PDCoV-infected IPI-2I cells, a line of more physiologically relevant intestinal epithelial cells to PDCoV infection *in vivo*. Here, we demonstrate that PDCoV enters IPI-2I cells via macropinocytosis, which does not require a specific receptor, and clathrin-mediated endocytosis, which requires a low-pH environment and dynamin, while a caveola-mediated endocytic pathway is used by PDCoV to enter swine testicular (ST) cells and porcine kidney (LLC-PK1) cells. These findings provide a molecular detail of the cellular entry pathways of PDCoV and may direct us toward novel antiviral drug development.

KEYWORDS porcine deltacoronavirus, endocytosis, clathrin, caveolae, macropinocytosis

Coronavirus (CoV) infections can cause respiratory illness and gastroenteritis in humans and animals. Several newly emerged coronaviruses have posed significant threats to public and animal health, including severe acute respiratory syndrome virus (SARS-CoV), Middle East respiratory syndrome virus, and the newly emerged SARS-CoV-2 in humans and the porcine deltacoronavirus (PDCoV) and swine enteric alphacoronavirus in animals (1–3). PDCoV belongs to the newly identified *Deltacoronavirus* genus in the *Coronavirus* family of

Citation Fang P, Zhang J, Zhang H, Xia S, Ren J, Tian L, Bai D, Fang L, Xiao S. 2021. Porcine deltacoronavirus enters porcine IPI-2I intestinal epithelial cells via macropinocytosis and clathrin-mediated endocytosis dependent on pH and dynamin. J Virol 95:e01345-21. https://doi.org/10.1128/JVI.01345-21.

Editor Tom Gallagher, Loyola University Chicago

Address correspondence to Shaobo Xiao, vet@mail.hzau.edu.cn.

Received 6 August 2021
Accepted 23 September 2021
Accepted manuscript posted online 29 September 2021
Published 23 November 2021

the *Nidovirales* order. PDCoV infection is characterized by acute diarrhea, vomiting, and mortality in nursing piglets, leading to considerable economic losses for the swine industry (4–6). PDCoV was first reported in Hong Kong in 2012 (7) and broke out in the United States in 2014 (8) and then rapidly spread to other countries (9–11), including China (12, 13). Several studies have indicated that PDCoV can also infect chickens (3), turkeys (14), and cattle (15). A recent study reported that PDCoV was identified in plasma samples of three Haitian children with acute undifferentiated febrile illness (16). These studies suggest that PDCoV possesses the potential for cross-species transmissibility (17), which has attracted increasing interest in studying this emerging coronavirus.

Viral entry into cells is the first step toward successful infection. Enveloped viruses enter cells either by directly fusing with the plasma membrane or by endocytic mechanisms. To date, several endocytic pathways used by viruses to enter host cells have been reported, such as clathrin-mediated endocytosis (CME), caveolae-mediated endocytosis (CavME), clathrin- and caveolae/raft-independent endocytosis, macropinocytosis, and lesser-known variations of these endocytic pathways (18). CME is the most evolutionarily conserved endocytic pathway and is extensively used by viruses; it is characterized by the uptake of cargo via invagination or clathrin-coated vesicles. African swine fever virus (ASFV), vesicular stomatitis virus (VSV), and rabies virus use the CME pathway to enter cells (19–21). In the classic CME pathway, low pH plays an essential role, and the dynamics of the endosomal system are modulated by Rab proteins, which are small GTPases of the Ras superfamily, including Rab5, Rab7, and Rab11, which are associated with selecting vesicle cargos, budding, targeting, and fusion. Evidence shows that these Rab proteins are involved in the life cycles of multiple viruses, including hepatitis C virus, dengue virus, and classical swine fever virus (CSFV) (22–24).

CavME, another well-characterized endocytic pathway, is a ligand-triggered process dependent on lipid rafts, dynamin, and a complex signaling pathway mediated by tyrosine kinase and phosphatase (25). Some viruses, including human coronavirus 229E (26), respiratory syncytial virus (27), and CSFV (23), are internalized via caveolae. Macropinocytosis is a regulated form of endocytosis that mediates nonselected uptake of solute molecules, nutrients, and antigens. Different from CME, macropinocytosis is involved in actin cytoskeleton reorganization, leading to the development of numerous irregular ruffles and blebs on the cell membrane (28). Influenza A virus (29), ASFV (30), and Ebolavirus (31) enter cells via macropinocytosis.

A previous study revealed that cholesterol in the cell membrane and viral envelope is essential for viral entry and replication (32). Zhang et al. further demonstrated that PDCoV enters cells through two pathways, one via cathepsin L (CTSL) and cathepsin B (CTSB) in the endosome, and another via a protease at the cell surface (33). However, how PDCoV enters host cells via endocytic pathways to initiate a successful infection remains uncertain and requires further study.

In this study, we initially used IPI-2I cells, a line of porcine intestinal epithelial cells derived from pig ileum, as a model to investigate PDCoV endocytosis. Specific pharmacological inhibitor treatment, immunofluorescence, small interfering RNA (siRNA) silencing, and overexpression of a dominant negative (DN) mutant results reveal that PDCoV entry into IPI-2I cells depends partially on the CME, requires a low pH and dynamin, and is independent of CavME. Apart from the CME pathway, macropinocytosis is another crucial endocytic pathway, dependent on the Na^+/H^+ exchanger (NHE). Additionally, depletion of Rab5 and/or Rab7, but not Rab11, impairs PDCoV infection, suggesting that viral transport from early to mature endosomes is an essential step in the PDCoV life cycle. In addition, the entry of PDCoV into other two porcine cell lines, swine testicular (ST) cells and porcine kidney (LLC-PK1) cells, was also assessed. We found that PDCoV enters ST and LLC-PK1 cells via a caveola-mediated endocytic pathway, independent of pH, the clathrin-mediated endocytosis pathway, and micropinocytosis, indicating that the pathways and strategies may be various for entry of PDCoV into different cell types. These results contribute greatly to the in-depth understanding of the PDCoV cellular entry pathways and provide new insights into antiviral drug development.

RESULTS

PDCoV entry into IPI-2I cells is dependent on a low pH. To investigate whether PDCoV entry is pH dependent, we evaluated the effect of two lysosomotropic agents, chloroquine and NH_4Cl, on PDCoV entry and infection in IPI-2I cells. The subtoxic doses of chloroquine were determined using a CCK-8-based cell viability assay, which showed that IPI-2I cells tolerated the chloroquine treatments up to 100 μM (Fig. 1A). Cells were pretreated for 1 h with various concentrations of chloroquine, followed by PDCoV infection for 1 h at 4°C (binding step), and then shifted to 37°C for 1 h (entry step). Viral RNA copy numbers were determined via reverse transcriptase quantitative PCR (RT-qPCR). As shown in Fig. 1B, chloroquine treatment inhibits PDCoV entry into cells but does not inhibit PDCoV binding to cells. At 6 h postinfection (hpi), viral infection was also evaluated using RT-qPCR, Western blot analysis, and 50% tissue culture infective dose ($TCID_{50}$) assay. Viral RNA copy numbers, N protein expression levels (Fig. 1C), and viral titer (Fig. 1D) were notably reduced dose-dependently after the chloroquine treatment. Immunofluorescence assay (IFA) was also performed to assess the effect of chloroquine on viral infection. Consistent with the results of RT-qPCR and Western blotting and viral titers, chloroquine treatment significantly and dose-dependently reduced the number of PDCoV-infected cells by approximately 28%, 26%, and 19% (the mean fluorescence intensities based on three independent experiments), respectively, compared to those of the dimethyl sulfoxide (DMSO)-treated control cells (Fig. 1E). Similar results were also observed in IPI-2I cells infected with PDCoV by NH_4Cl treatment (Fig. 1F to J). Previous studies showed that the internalizations of vesicular stomatitis virus (VSV) and Sendai virus (SeV) occur in a pH-dependent and pH-independent manner, respectively (19, 34, 35). Thus, we used VSV-green fluorescent protein (GFP) (a recombinant VSV expressing GFP) and SeV as the positive control and negative control, respectively. As shown in Fig. 1K and L, both chloroquine and NH_4Cl inhibited VSV-GFP entry into IPI-2I cells. However, no obviously negative effect of two components on SeV entry into IPI-2I cells was observed (Fig. 1M and N). These results strongly indicate that PDCoV requires a low pH to enter IPI-2I cells.

PDCoV enters IPI-2I cells via CME. Viruses can enter cells via endocytosis either dependently or independently of clathrin. To identify whether the endocytic pathways used by PDCoV involve clathrin, several complementary approaches were performed. Chlorpromazine (CPZ), a pharmacological inhibitor of clathrin lattice polymerization, was extensively used in previous studies (23, 36). Cell viability upon CPZ treatment was determined to exclude cytotoxic effects, and IPI-2I cell viability remained unchanged at up to 20 μM CPZ (Fig. 2A). The effect of CPZ on PDCoV entry and infection was evaluated via RT-qPCR and Western blotting. VSV-GFP serves as a positive control in this experiment. As shown in Fig. 2B, CPZ inhibits PDCoV entry but does not inhibit PDCoV binding. CPZ inhibits PDCoV and VSV-GFP infection in a dose-dependent manner, as evidenced by the results that RNA copy numbers and protein expression levels of the PDCoV N or GFP were notably reduced dose-dependently after CPZ treatment (Fig. 2C and D). Viral titer detection and IFA results indicated that CPZ treatment severely and dose-dependently inhibited PDCoV infection (Fig. 2E and 2F), consistent with the RT-qPCR and Western blotting results (Fig. 2C). EPS15 is reported to be a crucial component of clathrin-coated pits by interacting with adaptor protein 2, a major clathrin adaptor complex (37). The role of CME was further investigated by siRNA experiments. EPS15 knockdown significantly inhibited PDCoV entry into cells (Fig. 2G). At 6 hpi, viral infection was also evaluated using RT-qPCR and Western blot analysis. EPS15 knockdown significantly reduced viral RNA copy numbers and N protein expression levels, suggesting that EPS15 plays a positive role in PDCoV infection in IPI-2I cells (Fig. 2H). To further evaluate the role of clathrin in PDCoV internalization, clathrin heavy chain (CHC)-specific siRNA was used to knock down clathrin expression in IPI-2I cells, and then the cells were infected with PDCoV. Compared with the control siRNA, CHC siRNA notably inhibited PDCoV entry into IPI-2I cells (Fig. 2I). At 6 hpi, viral infection was also evaluated using RT-qPCR and Western blotting. CHC knockdown obviously reduced

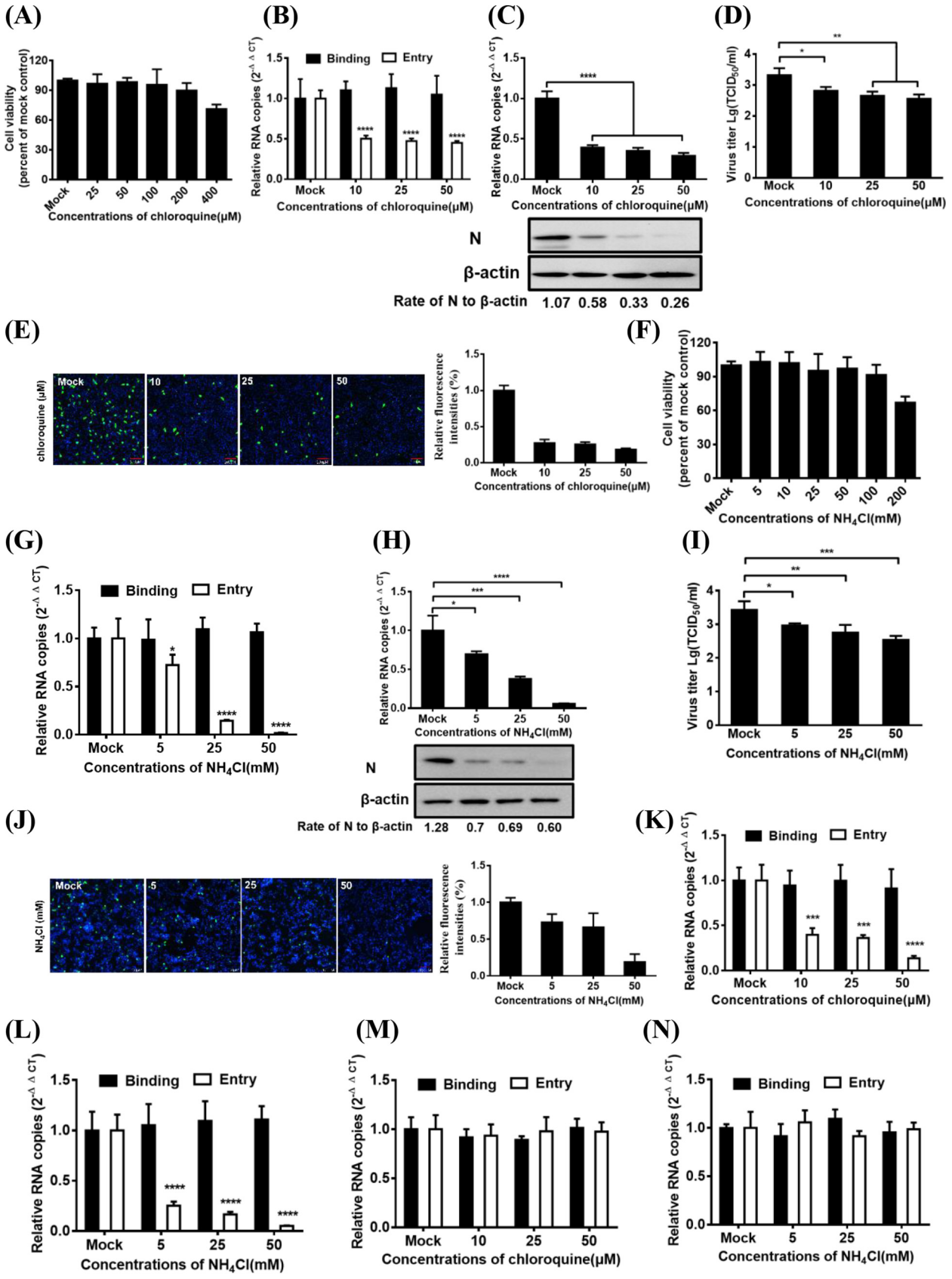

FIG 1 PDCoV entry into IPI-2I cells requires an acidic endosomal pH. (A) CCK-8-based cell viability assay for chloroquine as described in Materials and Methods. (B) Chloroquine inhibited PDCoV entry but not binding. IPI-2I cells were pretreated with subtoxic doses at 37°C for 1 h and infected

(Continued on next page)

CHC expression, viral RNA copy numbers, and N protein expression levels (Fig. 2J). These findings suggest that PDCoV entry into IPI-2I cells is clathrin dependent.

PDCoV entry into IPI-2I cells is caveola independent. Caveolae are cholesterol- and sphingolipid-rich smooth invaginations of the plasma membrane and are generally involved in caveolin, which is essential for caveolar formation and stability. The caveolin-mediated lipid raft-dependent pathway is a well-characterized endocytic pathway for SV40 entry (38). We therefore investigated whether caveolin-mediated endocytosis is vital to PDCoV internalization. IPI-2I cells were treated with various concentrations of nystatin (with known functions to disrupt the caveolar) (28) for 1 h, followed by PDCoV infection for 1 h at 4°C, and then shifted to 37°C for 1 h. Viral RNA copy numbers were determined via RT-qPCR. As shown in Fig. 3A, nystatin had an obvious detrimental effect on PDCoV binding and entry. At 6 hpi, viral infection was also evaluated by RT-qPCR and Western blotting. The results indicated that nystatin treatment failed to inhibit viral infection and instead slightly increased the viral RNA copy numbers and N protein expression levels (Fig. 3B). IPI-2I cell viability was also confirmed to be unchanged by concentration (10 and 25 μM; Fig. 3C). The role of the caveola was further investigated via expression of Flag-tagged DN caveolin-1 (Cav1) mutants (Cav1 DN, Cav1^{KSF}, and Cav1^{DGI}), followed by RT-qPCR, IFA, and Western blotting assay for the measurement of PDCoV entry and infection. Cav1 DN expression did not markedly affect PDCoV entry (Fig. 3D) and infection (Fig. 3E). Although the viral RNA copy numbers were slightly increased in cells expressing Cav1 DN compared with those expressing wild-type (WT) Cav1, N protein expression levels have no significant difference (Fig. 3F). Compared with the control siRNA, Cav1 siRNA knockdown did not have a significant effect on PDCoV entry into cells (Fig. 3G). At 6 hpi, viral infection was also evaluated using RT-qPCR and Western blotting. Cav1 siRNA effectively knocked down Cav1 expression but did not have a significant effect on viral RNA copy numbers and N protein expression levels (Fig. 3H). Taken together, these results strongly indicate that PDCoV entry into IPI-2I cells is caveola independent.

PDCoV entry into IPI-2I cells is dynamin dependent. Both clathrin and caveola-mediated endocytosis depend on dynamin 2, a large GTPase that is essential for vesicle scission during endocytosis (39). To determine whether dynamin is involved in PDCoV entry and infection, IPI-2I cells were treated for 1 h with increasing concentrations of dynasore, followed by PDCoV infection for 1 h at 4°C, and then shifted to 37°C for 1 h. Viral RNA copy numbers were determined via RT-qPCR. As shown in Fig. 4A, dynasore inhibited PDCoV entry but did not inhibit PDCoV binding. The infection of PDCoV or VSV-GFP was also evaluated further. RT-qPCR and Western blotting results showed that dynasore significantly reduced the PDCoV infection, just like the dose-dependent reduction of viral RNA and N protein levels (Fig. 4B). VSV-GFP infection was also attenuated dose-dependently but to a lesser degree than was PDCoV (Fig. 4C). The results of viral titer detection and IFA indicated that dynasore treatment severely and dose-dependently inhibited PDCoV infection (Fig. 4D and E). No cytotoxicity was observed in the cells treated with dynasore used in the experiments (Fig. 4F). These results showed that dynasore effectively impeded PDCoV endocytosis into IPI-2I cells. We further used RT-qPCR and confocal microscopy to investigate the

FIG 1 Legend (Continued)
with PDCoV (MOI of 5) at 4°C for 1 h (binding step) and then shifted to 37°C for 1 h (entry step). Cells were lysed to determine viral RNA copy numbers by RT-qPCR. (C and D) RT-qPCR, Western blotting, and viral titer detection analysis for viral infection inhibition by chloroquine. Cells were pretreated with increasing subtoxic doses of chloroquine or DMSO at 37°C for 1 h and then inoculated with PDCoV (MOI of 5) at 37°C for 6 h. Cells were lysed to determine viral RNA copy numbers via RT-qPCR, N protein levels via Western blotting (C), and viral titer (D) via $TCID_{50}$ assay. (E) IFA for viral infection inhibition by chloroquine. Cells were pretreated with subtoxic doses of these drugs at 37°C for 1 h and then inoculated with PDCoV (MOI of 5) at 37°C for 6 h. Cells were fixed and subjected to IFA. Relative fluorescence intensity was quantified by Image-Pro Plus software as shown on the right. (F) CCK-8-based cell viability assay for NH_4Cl as described in Materials and Methods. (G to J) RT-qPCR, Western blot analysis, viral titer detection, and IFA for viral entry and infection inhibition by NH_4Cl. Cells were pretreated with increasing subtoxic doses of NH_4Cl or H_2O, followed by RT-qPCR (G), Western blotting (H), viral titer detection (I), and IFA (J) as described in corresponding panels B, C, D, and E. (K to N) Effect of chloroquine and NH_4Cl on the entry of VSV-GFP and SeV into IPI-2I cells. The cells were pretreated with increasing subtoxic doses of chloroquine (K and M) or NH_4Cl (L and N) and then were infected with VSV-GFP (K and L) and SeV (M and N) at 4°C for 1 h (binding step) and then shifted to 37°C for 1 h (entry step). Cells were lysed to determine viral RNA copy numbers by RT-qPCR. Target protein expression was quantitatively estimated by ImageJ software and presented as the density value relative to that of the β-actin. The presented results represent the means and standard deviations of data from three independent experiments. *, $P < 0.05$; **, $P < 0.01$; ***, $P < 0.001$; ****, $P < 0.0001$.

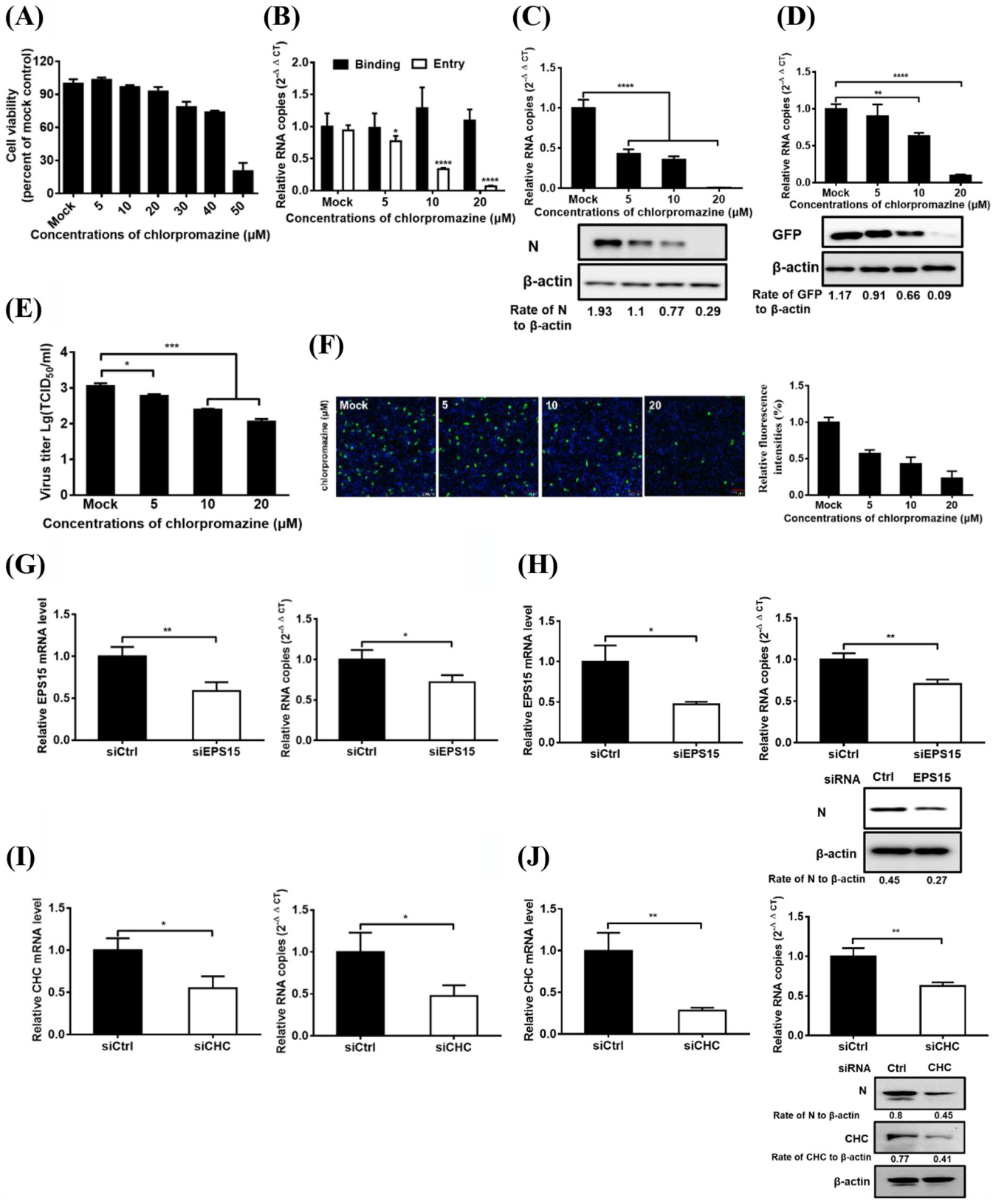

FIG 2 PDCoV entry into IPI-2I cells requires clathrin. (A) CCK-8-based cell viability assay for chlorpromazine as described in Materials and Methods. (B) Chlorpromazine inhibited PDCoV entry but not binding. IPI-2I cells were pretreated with subtoxic doses at 37°C for 1 h and infected with PDCoV (MOI of 5) at 4°C for 1 h (binding step) and then shifted to 37°C for 1 h (entry step). Cells were lysed to determine viral RNA copy numbers by RT-qPCR. (C and D) RT-qPCR and Western blot analysis for inhibition of PDCoV (C) and VSV-GFP (D) infections by chlorpromazine. Cells were pretreated with increasing subtoxic

(Continued on next page)

role of Flag-tagged DN dynamin mutants in PDCoV entry and infection, respectively. As shown in Fig. 4G, dynamin DN expression significantly inhibited PDCoV entry into cells compared to the control group. IFA results showed that IPI-2I cells expressing WT dynamin were infected with PDCoV, while cells expressing dynamin DN were barely infected with PDCoV (Fig. 4H). To further evaluate the role of dynamin in PDCoV internalization, an siRNA experiment was performed. Compared with the control siRNA, dynamin siRNA notably inhibited PDCoV entry and infection, as evidenced by the significantly reduced dynamin mRNA expression and viral RNA copy numbers (Fig. 4I and J). These results indicate that PDCoV entry into IPI-2I cells is dynamin dependent.

PDCoV entry into IPI-2I cells is macropinocytosis dependent. Macropinosome formation requires NHEs, which are considered a diagnostic criterion for macropinocytosis (40). To evaluate the role of macropinocytosis in PDCoV entry and infection, we examined the effect of 5-(*N*-ethyl-*N*-isopropyl) amiloride (EIPA; a macropinocytosis inhibitor that blocks Na^+/H^+ exchange) on PDCoV internalization and infection. As shown in Fig. 5A, EIPA inhibited PDCoV entry but did not inhibit PDCoV binding. Viral infection was evaluated by RT-qPCR, Western blotting, $TCID_{50}$, and IFA. EIPA treatment significantly decreased the PDCoV infection, just like the dose-dependent reduction of viral RNA levels, N protein levels (Fig. 5B), viral titer (Fig. 5C), and number of infected cells (Fig. 5D). Cell viability was unaffected by EIPA treatment at the concentrations used (Fig. 5E). Macropinocytosis also relied on phosphatidylinositol 3-kinase activation (41). Wortmannin, an inhibitor of this kinase, was used in subsequent experiments. Treating IPI-2I cells with the inhibitor had no obvious detrimental effect on PDCoV entry (Fig. 5F) and infection and even slightly increased the viral infection at the highest concentration used (Fig. 5G and H). Cell viability was also unaffected by wortmannin treatment at the concentration used (Fig. 5I). These findings suggest that PDCoV is internalized via macropinocytosis in IPI-2I cells.

Role of Rab proteins in PDCoV infection. To investigate the roles of small Rab5, Rab7, and Rab11 GTPases, key regulators in vesicular trafficking to early, late, and recycling endosomes, in PDCoV infection, several independent experiments were performed. DN mutants of Rab5 (S34N), Rab7 (T22N), and Rab11 (S25N) have been extensively reported in previous studies of enveloped viruses (23, 36). To determine whether blockage of Rab-mediated transport negatively affects viral infection, cells were transfected with WT Rab5, Rab7, Rab11, and their DN forms, then infected with PDCoV, followed by the detection of viral infection via IFA. IPI-2I cells overexpressing Rab5 DN and Rab7 DN, but not Rab11 DN, constructs were minimally infected with PDCoV compared with cells overexpressing WT Rab5 and Rab7 (Fig. 6A), indicating that Rab5 and Rab7 are required for PDCoV transportation after internalization. To further identify the endosomal compartment traversed by endocytosed PDCoV, Rab5-, Rab7-, and Rab11-specific siRNAs were used to examine the requirement of transportation to the endosomes in PDCoV entry. The silencing efficiencies of siRab5, siRab7, and siRab11 were determined via RT-qPCR and Western blot analysis (Fig. 6B to D). Compared with control siRNA, Rab5 and Rab7 siRNA notably reduced viral RNA copy numbers and N protein expression levels (Fig. 6B and C). Consistent with the IFA results, cells transfected with Rab11 siRNA had no obvious detrimental effect on viral infection compared with that of the negative control (Fig. 6D). These results suggest that Rab5 and Rab7 are required for PDCoV endocytosis and subsequent productive infection.

FIG 2 Legend (Continued)
doses of chlorpromazine or DMSO at 37°C for 1 h and then inoculated with VSV-GFP or PDCoV (MOI of 5) at 37°C for 6 h. Cells were lysed to determine viral RNA copy numbers via RT-qPCR and viral protein levels via Western blotting. (E) Viral titer detection for PDCoV in the medium from cells treated as described in panel C. (F) IFA for viral infection inhibition by chlorpromazine. Cells were pretreated as described in panel C, followed by IFA using anti-PDCoV N antibody. Relative fluorescence intensity is quantified by Image-Pro Plus software as shown in panel F on the right. (G and H) EPS15 knockdown inhibited PDCoV entry (G) and infection (H). siEPS15- or siCtrl-transfected cells were infected with PDCoV (MOI of 5). At 1 and 6 hpi at 37°C, cells were lysed to determine the silencing efficiency of EPS15, the viral RNA copy numbers via RT-qPCR, and N protein expression levels by Western blotting. (I and J) CHC knockdown inhibited PDCoV entry (I) and infection (J). siCHC- or siCtrl-transfected cells were infected with PDCoV (MOI of 5). At 1 and 6 hpi at 37°C, the cells were lysed to determine the viral RNA copy numbers and N protein expression levels via RT-qPCR and Western blot analysis, respectively. Target protein expression was quantitatively estimated by ImageJ software and presented as the density value relative to that of the β-actin. The presented results represent the means and standard deviations of data from three independent experiments. *, $P < 0.05$; **, $P < 0.01$; ***, $P < 0.001$; ****, $P < 0.0001$.

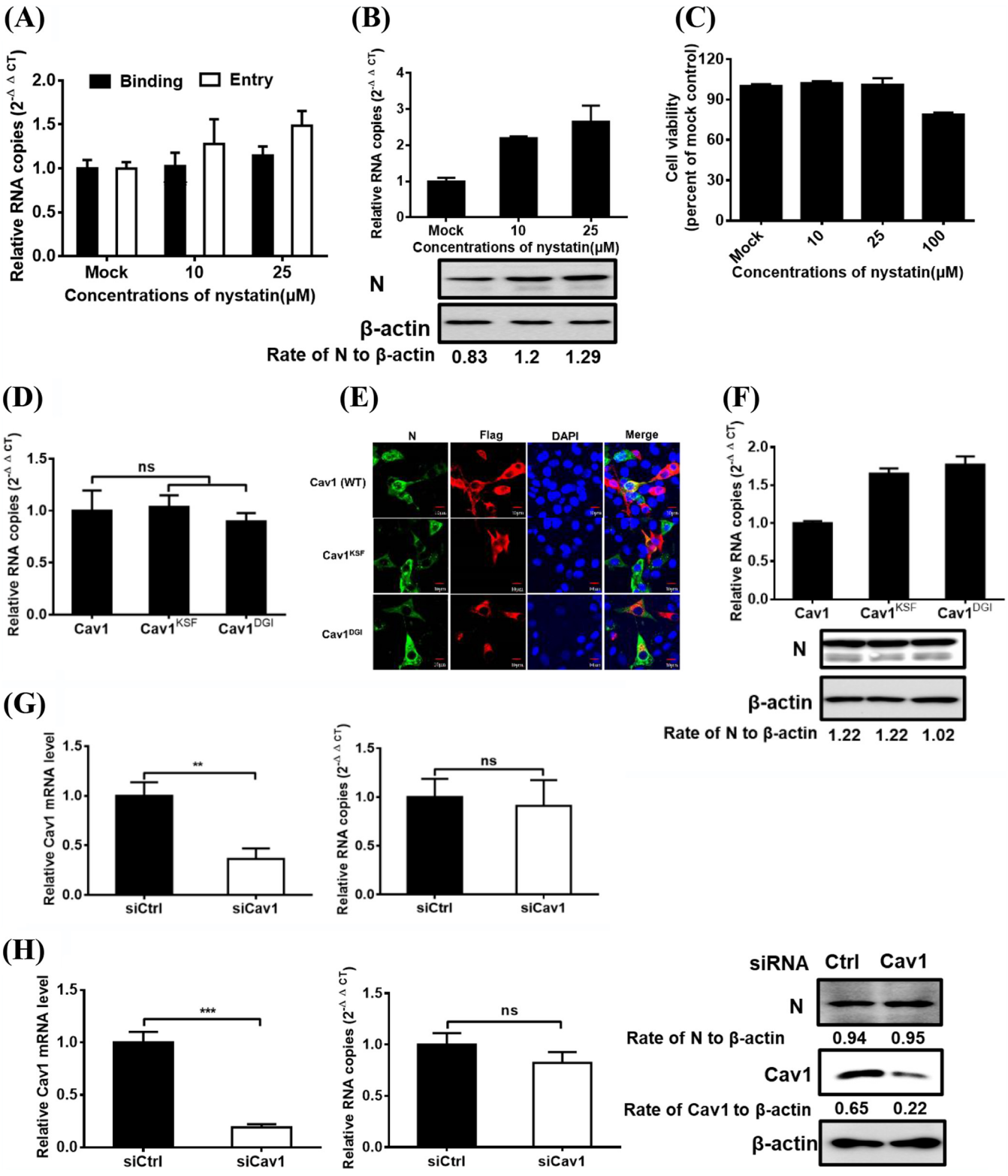

FIG 3 Caveolae are not required for PDCoV entry into IPI-2I cells. (A) Effect of nystatin on PDCoV binding and entry. IPI-2I cells were pretreated with increasing subtoxic doses at 37°C for 1 h and infected with PDCoV (MOI of 5) at 4°C for 1 h (binding step) and then shifted to 37°C for 1 h (entry step). Cells were lysed to determine viral RNA copy numbers by RT-qPCR. (B) RT-qPCR and Western blot for inhibition of PDCoV infection by nystatin. Cells were pretreated with increasing subtoxic doses of nystatin or DMSO at 37°C for 1 h and then inoculated with PDCoV (MOI of 5) at 37°C for 6 h. Cells were lysed to determine viral RNA copy numbers via RT-qPCR and N protein levels via Western blot analysis. (C) CCK-8-based cell viability assay for nystatin as described in Materials and Methods. (D to F) Effect of DN caveolin (Cav1) on PDCoV entry (D) and infection (E and F) was determined via RT-qPCR, confocal microscopy, and Western blot analysis. Cells transfected with plasmid constructs encoding Flag-tagged WT and DN Cav1 were infected with PDCoV (MOI of 5).

(Continued on next page)

The pathways used by PDCoV to enter other porcine cell lines. Many studies have indicated that a virus may enter into different cell types via different pathways. Therefore, we further investigated the pathways used by PDCoV to enter two other porcine cell lines, ST and LLC-PK1 cells. No obvious cytotoxic effects could be detected in both ST and LLC-PK1 cells when the highest concentrations of several key inhibitors used in IPI-2I cells were used (data not shown), and the effects of several key inhibitors on the entry of PDCoV into ST and LLC-PK1 cells were determined via RT-qPCR. As shown in Fig. 7A, for ST cells, chloroquine, NH_4Cl, chlorpromazine, EIPA, and wortmannin treatments did not obviously inhibit the viral RNA copy numbers compared with those in DMSO- or H_2O-treated control cells, while nystatin treatment significantly inhibited the viral RNA copy numbers compared with those in control cells. Similar results were also observed in LLC-PK1 cells (Fig. 7B). These results showed that, different from the entry pathway in IPI-2I cells, PDCoV enters ST and LLC-PK1 cells via a caveola-mediated endocytic pathway, independent of pH, the clathrin-mediated endocytosis pathway, and macropinocytosis. Taken together, these results indicated that PDCoV enters different cell types via distinct pathways and strategies.

DISCUSSION

PDCoV enters cells through both direct membrane fusion at the cell surface and endocytic pathways (33, 42). Endocytic pathways are the most widely reported entry approach used by numerous viruses. Therefore, we mainly focused on the entry of PDCoV via endocytic pathways and systematically investigated the steps of this process. Our results reveal that PDCoV entry into IPI-2I cells depends on macropinocytosis and the CME, requires low pH and dynamin, and is independent of CavME. Furthermore, Rab5 and Rab7, but not Rab11, are required for PDCoV infection.

Accumulating evidence shows that the entry processes of many viruses, including coronaviruses, via endocytic uptake often require an acidic endosomal environment to undergo uncoating and/or escape from the endosome and the decline of local pH, followed by internalization into endolysosomes. Using chloroquine and NH_4Cl that selectively enhance the luminal pH of the endosome and lysosome, we first demonstrated that PDCoV enters IPI-2I cells dependent on a low-pH microenvironment, suggesting endocytic uptake and viral delivery to an acidic intracellular compartment where fusion occurs. In addition, we chose VSV-GFP and SeV as the positive and negative controls in this study, respectively. As expected, chloroquine and NH_4Cl inhibited VSV-GFP entry into IPI-2I cells but did not have a significant negative effect on SeV entry. These results suggested that their inhibitory effects on PDCoV entry into IPI-2I cells was not due to the general cytotoxicity of the drugs, which strongly supports that PDCoV entry into IPI-2I cells is dependent on a low pH. This conclusion is consistent with a previous report that bafilomycin A1, a lysosomal acidification inhibitor that blocks vacuolar proton ATPases, significantly inhibited PDCoV infection (33). In this study, combining approaches of CPZ-mediated inhibition and clathrin heavy-chain knockdown, we provided a direct support that PDCoV entry into IPI-2I cells depends on clathrin. Many studies have indicated that clathrin-mediated entry of viruses, such as porcine hemagglutinating encephalomyelitis virus, Japanese encephalitis virus (JEV), and CSFV, depends on EPS15 (36, 43, 44). However, mouse hepatitis virus type 2 entry reportedly occurred through a CME pathway independent of EPS15. Here, we showed that the CME pathway of PDCoV depends on EPS15. Dynamin is a high-molecular-weight GTPase that mediates membrane fusion required for clathrin-mediated endocytosis. In this study, the essential role of dynamin in the PDCoV entry into IPI-2I cells process was further

FIG 3 Legend (Continued)
At 1 and 6 hpi at 37°C, cells were harvested and subjected to RT-qPCR, IFA, and Western blot analysis, respectively. Bar, 10 μm. (G and H) Cav1 knockdown failed to inhibit PDCoV entry (G) and infection (H). siCav1- or siCtrl-transfected cells were infected with PDCoV (MOI of 5). At 1 and 6 hpi at 37°C, the cells were lysed to determine the silencing efficiency of Cav1, the viral RNA copy numbers, and N protein expression levels via RT-qPCR and Western blot analysis. Target protein expression was quantitatively estimated by ImageJ software and presented as the density value relative to that of the β-actin. The presented results represent the means and standard deviations of data from three independent experiments. **, $P < 0.01$; ***, $P < 0.001$; ns, nonsignificant difference.

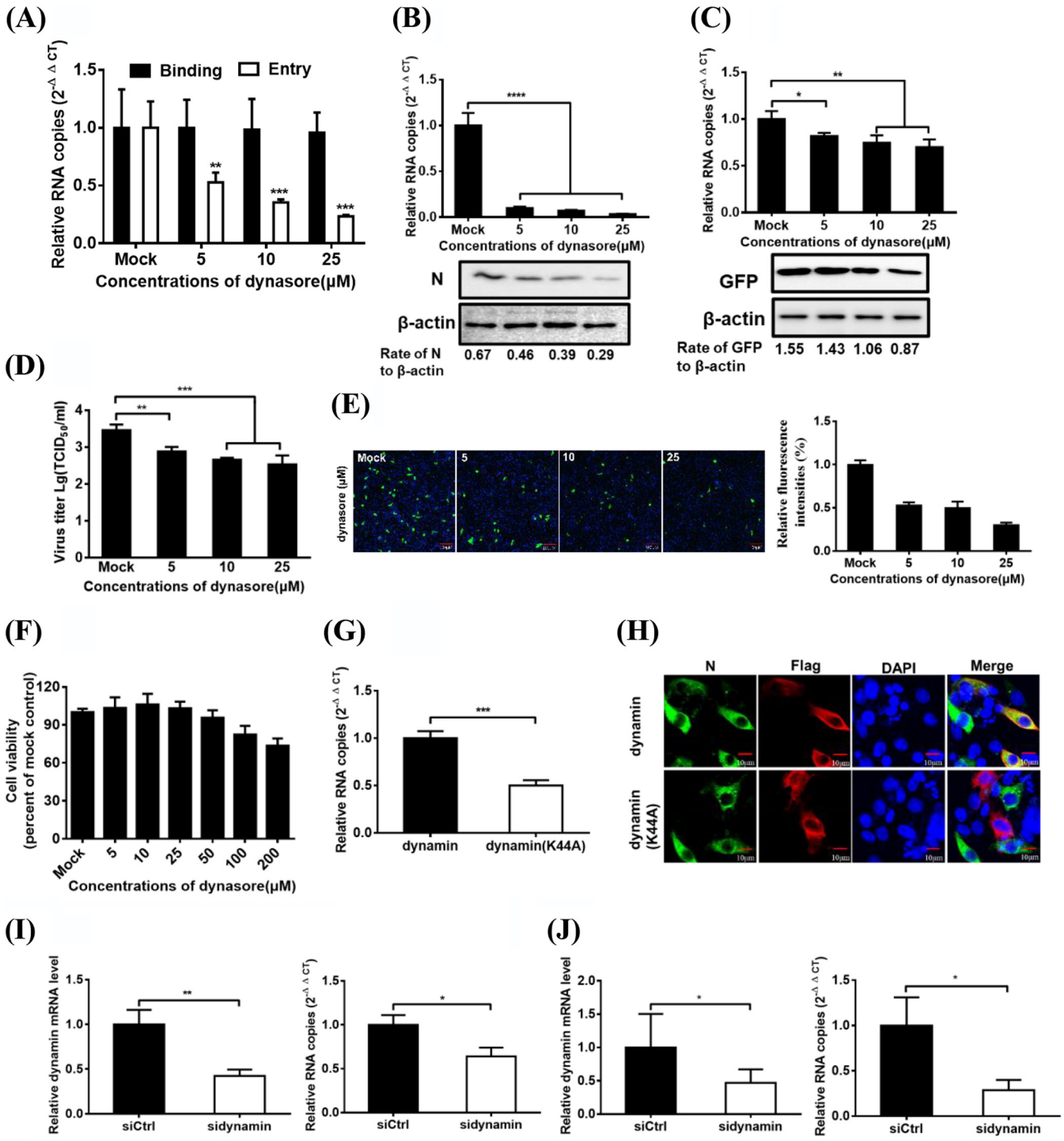

FIG 4 PDCoV entry into IPI-2I cells depends on dynamin. (A) Effect of dynasore on PDCoV binding and entry. IPI-2I cells were pretreated with increasing subtoxic doses as described in above Fig. 3A, and lysed cells were subjected to determine viral RNA copy numbers by RT-qPCR. (B and C) Dynasore inhibited PDCoV and VSV-GFP infection. Cells were pretreated with increasing subtoxic doses of dynasore or DMSO at 37°C for 1 h and then inoculated with PDCoV (B) or VSV-GFP (C) at 37°C for 6 h, followed by determination of viral infection by RNA copy numbers and viral protein expression levels by RT-qPCR and Western blot analysis. (D) Viral titer detection for PDCoV in the medium from cells treated as described in panel B. (E) IFA for the effect of dynasore on PDCoV infection. Cells were pretreated as described in panels B, followed by IFA. Bar, 100 μm. Relative fluorescence intensity is quantified by Image-Pro Plus software as shown in panel E on the right. (F) CCK-8-based cell viability assay for dynasore as described in Materials and Methods. (G and H) Inhibitory effect of the dynamin DN construct on PDCoV entry (G) and infection (H) was determined via RT-qPCR and confocal microscopy. Cells transfected with plasmid constructs encoding Flag-tagged WT and DN dynamin were infected with PDCoV (MOI of 5). At 1 and 6 hpi at 37°C, cells were harvested and subjected to RT-qPCR and IFA, respectively. Bar, 10 μm. (I and J) Dynamin knockdown inhibited PDCoV entry (I) and infection (J). Si-dynamin- or siCtrl-transfected cells were infected with PDCoV (MOI of 5). At 1 and 6 hpi at 37°C, the cells were lysed to determine the viral RNA copy numbers via RT-qPCR. Target protein expression was quantitatively estimated by ImageJ software and presented as the density value relative to that of the β-actin. The presented results represent the means and standard deviations of data from three independent experiments. *, $P < 0.05$; **, $P < 0.01$; ***, $P < 0.001$; ****, $P < 0.0001$.

determined (Fig. 4). CME is a primarily receptor-mediated pathway. However, to date, the key functional receptor of PDCoV remains unknown. Several studies have indicated that aminopeptidase N (APN), a receptor of several alphacoronaviruses, promotes susceptibility to PDCoV infection in nonsusceptible cells (17, 45) but is likely not a functional receptor owing to normal viral infection in APN-knockout cells *in vitro* and *in vivo* (46–48). Whether the increase in APN-mediated PDCoV infection depends on clathrin requires further investigation.

A previous study showed that PDCoV production was limited when cells were treated with methyl-beta-cyclodextrin (MβCD) prior to infection and was almost abolished when cholesterol was depleted from the viral envelope (32). This suggests that lipid rafts and cholesterol-enriched lipid-order membranes play crucial roles in PDCoV entry into cells. To define the role of caveola-mediated endocytosis in PDCoV entry into IPI-2I cells, we used nystatin, a polyene antifungal agent that interacts with cholesterol and inhibits the lipid raft/caveolin pathway. In our experiment, nystatin treatment could not block and even slightly promote viral infection, suggesting that inhibition of PDCoV entry via depletion of cholesterol by MβCD did not occur by impairing caveola-mediated endocytosis but likely by disturbing the integrity of the membrane lipid microdomains. Similar results have been reported for SARS-CoV (49), foot-and-mouth disease virus (28), and JEV (36). Entry of these viruses into cells did not depend on caveolae but required the involvement of cholesterol. Different from the entry pathway in IPI-2I cells, PDCoV enters ST and LLC-PK1 cells via a caveola-mediated endocytic pathway, independent of pH, the clathrin-mediated endocytosis pathway, and macropinocytosis as evidenced by the significantly lower PDCoV internalization level due to nystatin treatment, and no obvious effects by chloroquine, NH_4Cl, CPZ, EIPA, and wortmannin compared with the control group (Fig. 7). PDCoV replicates so efficiently in ST and LLC-PK1 cells, implying that both two cell lines possess cellular receptors for PDCoV entry. In addition, the caveola-mediated endocytosis is ligand triggered and characterized by the formation of primary endocytic vesicles. It depends on cholesterol, lipid rafts, and a complex signaling pathway associated with tyrosine kinase and phosphatases (50). It is possible that nystatin treatment disrupts the formation or stability of caveola, which consists of potential PDCoV receptor molecules or coreceptors and subsequently interferes with PDCoV entry, but it needs to be further investigated. These results indicated that PDCoV may enter different cell types via different pathways. It should be noted that similar phenomena had been reported in other viruses, including coronaviruses. For example, CSFV enters into porcine alveolar macrophages dependent on pH, dynamin, and caveola-mediated pathway (23), but enters into PK-15 cells via clathrin-mediated endocytic pathway (44). JEV enters into PK-15 cells via clathrin-mediated pathways, independent of pH and the caveola-mediated pathway (44, 51), while JEV enters into rat neuroblastoma cells via a pH-dependent, dynamin- and caveola-mediated endocytosis pathway (52). A recent study indicated that Newcastle disease virus (NDV) enters into chicken origin cells (HD11 and LMH) via a pH-dependent, dynamin- and caveola-mediated endocytic pathway, while NDV enters into DF-1 cells via pH-dependent dynamin, the clathrin-mediated endocytosis pathway, as well as macropinocytosis (53). Currently, there are relatively few studies on the enter pathways of coronaviruses in different cells. However, SARS-CoV has been reported to enter the hepatocellular carcinoma cell line HepG2 through clathrin-mediated endocytosis (54), while it enters Vero cells through a clathrin- and caveolae-independent endocytic pathway (49), suggesting that coronaviruses can use different pathways to enter different cells, and our present study further supports this conclusion.

Macropinocytosis is characterized by actin-dependent membrane ruffling, is thought to be independent of receptors or dynamin (31), and is the only endocytic pathway sensitive to NHE deactivation. EIPA is often reported to be a main indicator of viral macropinocytosis. Here, EIPA notably impeded PDCoV entry into IPI-2I cells dose-dependently, while the phosphatidylinositol 3-kinase (PI3K) inhibitor wortmannin did not, suggesting that macropinocytosis-mediated PDCoV entry into IPI-2I cells depends on NHE and is independent of the PI3K pathway. In addition to NHE and PI3K, Rho GTPases (Rac1 and Cdc42), kinases (Pak1 and

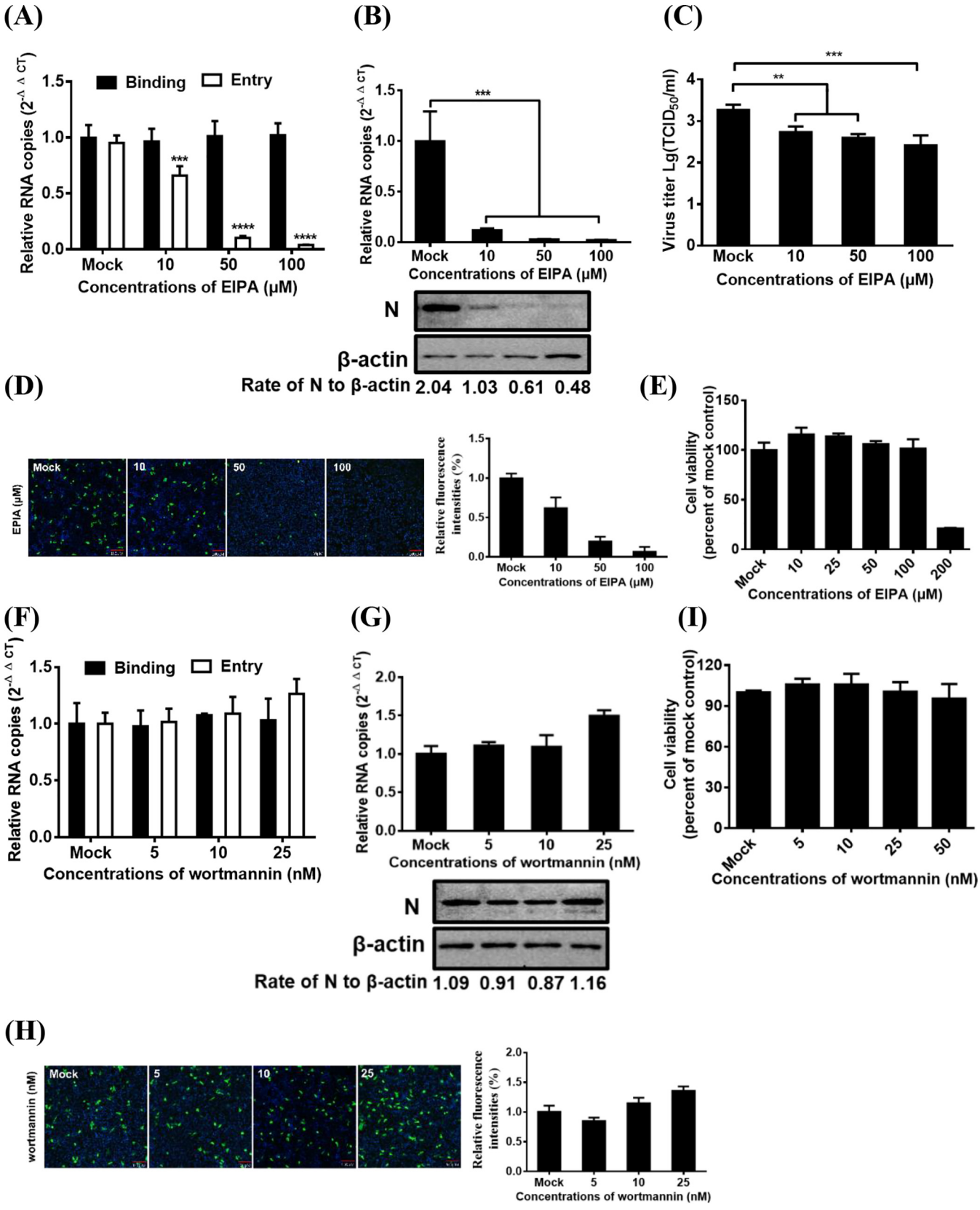

FIG 5 PDCoV entry into IPI-2I cells depends on macropinocytosis. (A and F) Effect of EIPA (A) and wortmannin (F) on PDCoV binding and entry. IPI-2I cells were pretreated with increasing subtoxic doses as described in above Fig. 3A, and lysed cells were subjected to determine viral RNA copy numbers by RT-qPCR. (B and G) RT-qPCR and Western blot analysis for the effect of EIPA (B) and wortmannin (G) on PDCoV infection. Cells were pretreated with increasing

(Continued on next page)

PKC), and myosin II are associated with macropinocytosis. PKC is a $Ca2^{+}$- and diacylglycerol-dependent serine/threonine kinase, and its activation promotes formation of membrane ruffles and macropinosomes (55). Our previous study demonstrated that PDCoV modulates calcium influx to favor viral replication (56). Therefore, PDCoV may modulate calcium signaling to result in macropinocytosis, which requires further investigation. In this study, we did not further investigate whether other pathways were involved in macropinocytosis-mediated PDCoV entry into IPI-2I cells. Previous studies have shown that PDCoV infects various host cells, including pigs, chickens, cattle, and humans (3, 15), suggesting its extensive host tropism. Macropinocytosis acts as an alternative approach for PDCoV entry into cells, which may expand the cellular range of PDCoV and might explain the replication of PDCoV in APN-negative lung fibroblast-like cells and porcine alveolar macrophages (PAMs) (47, 48), but it needs to be further verified through additional experiments. In addition, the molecular details of macropinocytosis used by PDCoV to enter IPI-2I cells require further study.

Rab5 and Rab7 GTPases are key regulators of transport to early and late endosomes, the role of which has been extensively investigated in viral entry (23, 44). Rab9 facilitates vesicular transport from the late-endosome to the *trans*-Golgi network (57). Rab11 is localized primarily to perinuclear recycling endosomes and modulates a slower recycling pathway via these compartments. Accumulating evidence indicated that entry of some members of *Flaviviridae*, including JEV, CSFV, and West Nile virus, into cells depends on Rab5, or/and Rab7, or/and Rab11 (22, 23, 36, 44). However, studies on the roles of Rab proteins in coronavirus infections remain largely unclear. PEDV entry into cells is reported to depend on the endolysosome pathway, which is involved in Rab7 (58). RNAi (RNA interference)-mediated gene silencing identified endocytosis-associated proteins, including early endosome-associated genes (EEA1 and Rab5), late endosome-associated genes (Rab7A and Rab7B), and late-endosome to lysosome maturation-associated genes (VPS39), to be important for mouse hepatitis virus (MHV) infection (59). In addition, functional inactivation of Rab5 and Rab7 obviously inhibited infectious bronchitis virus (IBV) infection (60). These data showed that Rab5, Rab7, or Rab11 appears to be more important for virus transport. Here, overexpression of DN Rab proteins and RNAi technology showed that Rab5 and Rab7 are required for the trafficking of PDCoV particles following endocytosis. Late endosome to lysosome maturation was not monitored in this study, but a previous study demonstrated that lysosomal CTSL and CTSB facilitated PDCoV entry into cells, suggesting that the endolysosomal pathway is also involved in PDCoV endocytosis (33). Therefore, we hypothesized that PDCoV particles are first transported to early endosomes in a Rab5-dependent manner and then guided to late endosomes via a Rab7-dependent pathway. PDCoV is then transported to the lysosome and processed by lysosomal proteases, such as CTSL and CTSB, to release viral RNA. Several coronaviruses, such as mouse hepatitis virus (MHV) and feline infectious peritonitis virus (FIPV), use this classic endocytic pathway (59). Interestingly, these viruses can modulate the endolysosomal system to facilitate the fusion of viral and endosomal membranes and subsequent release of the viral genome into the cytosol and to escape degradation by the acidic environment and various enzymes. The detailed molecular mechanisms deserve further exploration.

In conclusion, our results demonstrate that PDCoV enters IPI-2I cells via clathrin-dependent endocytosis and macropinocytosis. After endocytosis, PDCoV is transported from early to late endosomes and then likely to the lysosomes before an acidic pH-

FIG 5 Legend (Continued)
subtoxic doses of these drugs or DMSO at 37°C for 1 h and then inoculated with PDCoV at 37°C for 6 h, followed by determination of viral infection by RNA copy numbers and viral protein expression levels via RT-qPCR and Western blot analysis. (C) Viral titer detection for PDCoV in the medium from cells treated as described in panel B. (D and H) IFA for the effects of EIPA (D) and wortmannin (H) on PDCoV infection. Cells were treated as described in panels B and G, respectively. Infected cells were fixed and subjected to IFA using anti-PDCoV N antibody as the primary antibody. Relative fluorescence intensity is quantified by Image-Pro Plus software as shown in panels D and H on the right. (E and I) CCK-8-based cell viability assay for EIPA (E) and wortmannin (I) as described in Materials and Methods. Target protein expression was quantitatively estimated by ImageJ software and presented as the density value relative to that of the β-actin. The presented results represent the means and standard deviations of data from three independent experiments. **, $P < 0.01$; ***, $P < 0.001$.

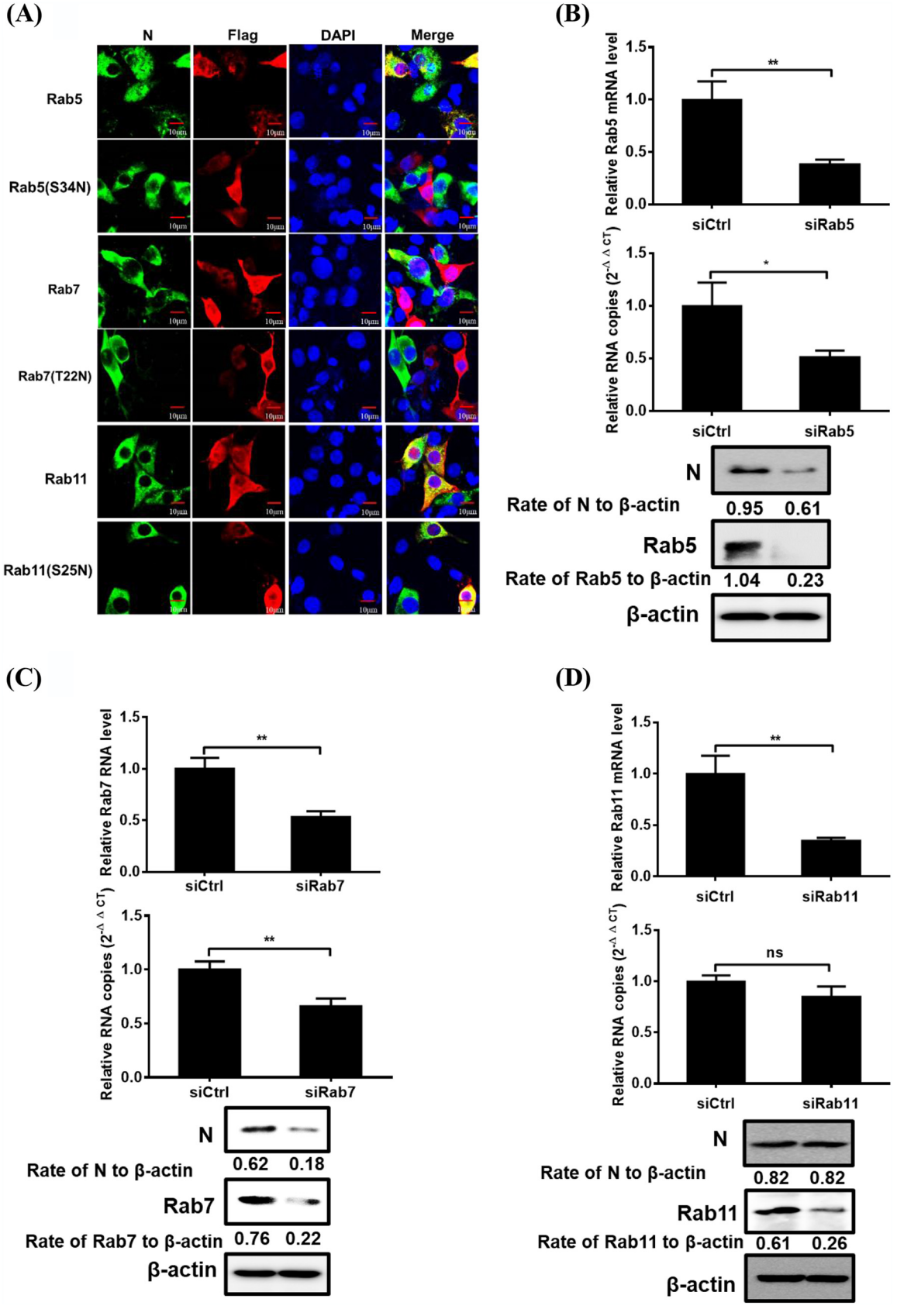

FIG 6 Effect of Rabs on PDCoV infection. (A) Effect of DN Rab proteins on PDCoV infection was determined via confocal microscopy. Cells transfected with plasmid constructs encoding Flag-tagged Rab5, Rab7, Rab11 WT, or DN were infected with PDCoV (MOI of 5)

(Continued on next page)

dependent step, followed by the release of viral RNA to the cytoplasm and subsequent successful infection.

MATERIALS AND METHODS

Viruses, cells, and antibodies. IPI-2I cells were obtained from the China Center for Type Culture Collection and were cultured and maintained at 37°C and 5% CO_2 in Dulbecco's modified Eagle's medium (DMEM; Invitrogen, NY, USA) supplemented with 10% heat-inactivated fetal bovine serum (Pan-Biotech, Bavaria, Germany). ST and LLC-PK1 cells were purchased from American Type Culture Collection (ATCC CL-101). PDCoV strain CHN-HN-2014 (GenBank accession number KT336560) was isolated from a piglet with severe diarrhea in China in 2014 (2). SeV was obtained from the Centre of Virus Resource and Information, Wuhan Institute of Virology, Chinese Academy of Sciences. Vesicular stomatitis virus expressing green fluorescent protein (VSV-GFP) was gifted by Zhigao Bu at Harbin Veterinary Research Institute, Chinese Academy of Agricultural Sciences. Rabbit anti-Cav1, anti-CHC, anti-Rab5, anti-Rab7, and anti-Rab11 antibodies were purchased from Cell Signaling Technology (Danvers, MA, USA). Mouse anti-Flag and anti-GFP antibodies were purchased from Medical and Biological Laboratories (Nagoya, Japan). Mouse anti-PDCoV N antibody was described previously (61).

RNA extraction and quantitative real-time RT-PCR. Cells in 24-well plates were treated with various experimental conditions, followed by PDCoV, VSV-GFP, or SeV infection. At the indicated time points, total RNA was extracted from the cells using TRIzol reagent (Invitrogen), followed by first-strand cDNA synthesis using avian myeloblastosis virus reverse transcriptase (TaKaRa, Japan) with the indicated primers (Table 1). The cDNA was used as the templates and subjected to SYBR green PCR assays (Applied Biosystems) at least three times. The results are expressed as threshold cycle ($2^{-\Delta\Delta CT}$) from quadruplicate samples. Glyceraldehyde-3-phosphate dehydrogenase was used as the reference gene.

Cell infection and drug treatment. To determine the effects of various drugs on the PDCoV infection, cells grown to 90% confluence were treated with the indicated concentrations in figures of chloroquine (MedChemExpress [MCE], NJ, USA), NH_4Cl (Sigma), chlorpromazine (CPZ; MCE), dynasore (MCE), wortmannin (MCE), or 5-(*N*-ethyl-*N*-isopropyl) amiloride (EIPA; MCE) for 1 h at 37°C before or during PDCoV infection. For the PDCoV binding and internalization, cells were infected at a multiplicity of infection (MOI) of 5 in the presence of these drugs at 4°C for 1 h, during when viruses can bind cells but no entry can occur (binding step), and then shifted to 37°C for 1 h, during when viruses start to enter cells (entry step). Cellular total RNA was extracted using TRIzol reagent, followed by the measurement of viral genomic RNA (gRNA) via RT-qPCR with specific primers (Table 1) targeting the nsp16 gene of PDCoV as described previously (46).

Cell viability analysis. The cytotoxic effects of the drugs on cells were measured using a CCK-8-based cell viability assay (Beyotime, Shanghai, China). Briefly, cells were treated with various concentrations of the indicated drugs for 12 h and then subjected to CCK-8-based cell viability assays according to the manufacturer's instructions. No cytotoxicity was observed in the cells treated with the indicated concentrations of these drugs.

Plasmids and siRNA transfections. The full-length cDNA of dynamin-2 and Cav1 was amplified from IPI-2I cells using the indicated primers (Table 1) and then cloned into pCAGGS-Flag-N with an N-terminal Flag tag to yield pCAGGS-Flag-dynamin-2 and pCAGGS-Flag-Cav1, respectively. Dynamin-2 DN (K44A) form was constructed by mutagenesis of amino acid (aa) 44 K to A. Two DN forms of Cav1, $Cav1^{KSF}$ (aa 135 to 178) and $Cav1^{DGI}$ (aa 82 to 178), were constructed as previously described (62). Flag-tagged expression constructs encoding wild-type (WT) Rab5 and DN Rab5 (S34N), WT Rab7 and DN Rab7 (T22N), and WT Rab11 and DN Rab11 (S25N) were constructed by cloning the corresponding full-length cDNA into the pCAGGS-Flag-N vector with the indicated primers (Table 1) using GFP-WT Rab5 and GFP-DN Rab5 (S34N), GFP-WT Rab7 and GFP-DN Rab7 (T22N), or GFP-WT Rab11 and GFP-DN Rab11 (S25N) expression plasmids gifted from Stephen S. G. Ferguson at the University of Ottawa as the templates.

To investigate the effect of the DN mutants on PDCoV infection, cells on coverslip dishes with 80% confluence were transfected with the indicated expression plasmids using Lipofectamine 3000 (Invitrogen) according to the manufacturer's instructions. For the siRNA interference experiment, IPI-2I cells were seeded in 24-well plates with 80% confluence and then transfected with siRNA using Lipofectamine 3000. The siRNA duplexes included siEPS15, siCHC, siCav1, sidynamin, siRab5, siRab7, siRab11, and the negative-control siCtrl (Table 2). After 24 h of transfection, cells were infected with PDCoV at an MOI of 5 at 4°C for 1 h and then shifted to 37°C for 1 h or 6 h. PDCoV entry and infection were evaluated via RT-qPCR, Western blotting, or confocal fluorescence microscopy.

FIG 6 Legend (Continued)
at 37°C for 6 h. Cells were fixed with 4% paraformaldehyde and then reacted with anti-Flag and anti-PDCoV N antibodies and visualized via confocal microscopy. Bar, 10 μm. (B to D) Rab5 and Rab7, but not Rab11, knockdown inhibited PDCoV infection. siRab5- (B), siRab7- (C), siRab11- (D), or siCtrl-transfected cells were infected with PDCoV (MOI of 5) for 6 h. Cells were lysed to determine the silencing efficiency of Rabs, viral RNA copy numbers, and N protein expression levels via RT-qPCR and Western blot analysis. Target protein expression was quantitatively estimated by ImageJ software and presented as the density value relative to that of the β-actin. The presented results represent the means and standard deviations of data from three independent experiments. *, $P < 0.05$; **, $P < 0.01$; ns, nonsignificant difference.

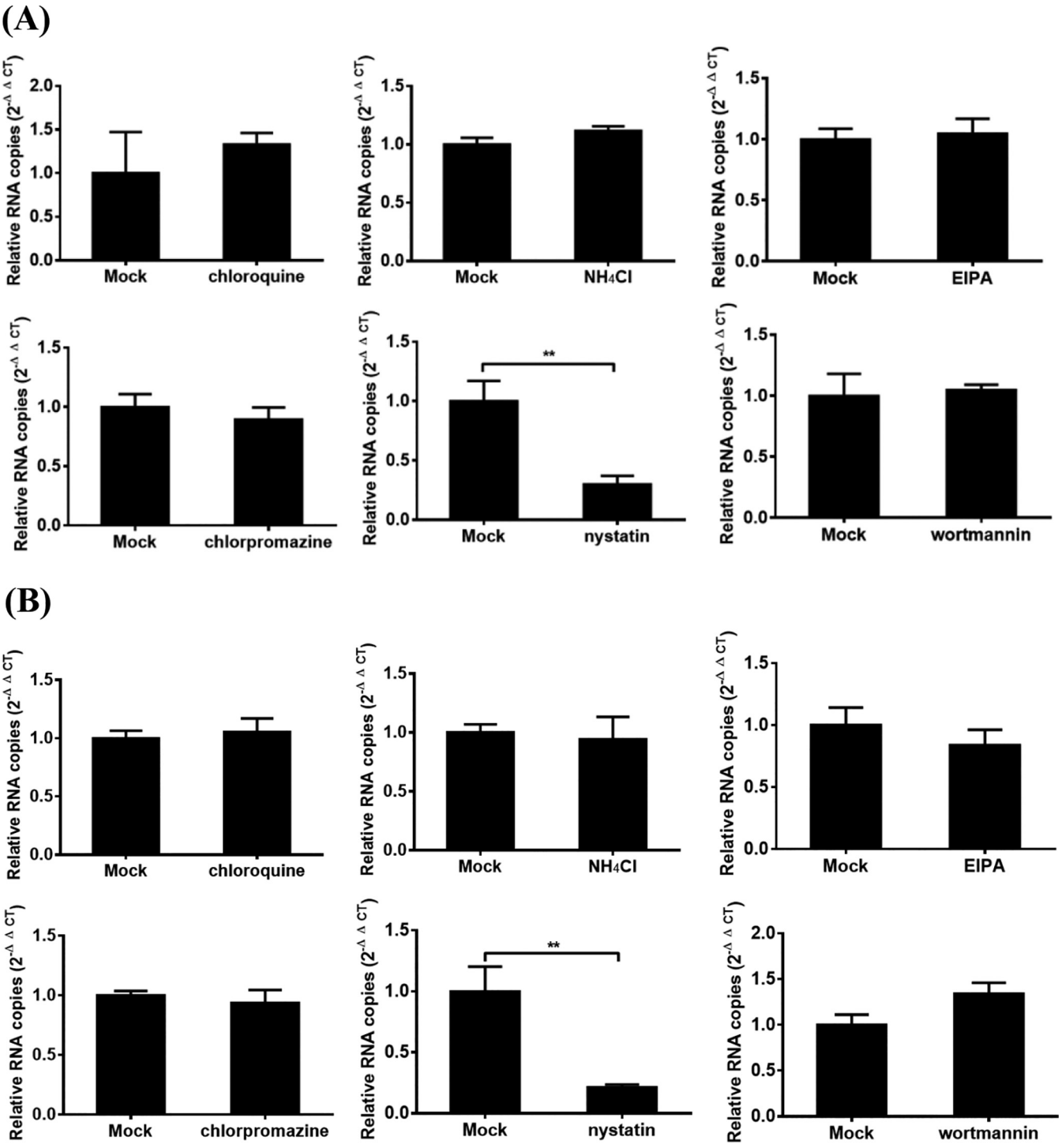

FIG 7 Effects of inhibitors on the entry of PDCoV into ST and LLC-PK1 cells. (A and B) ST (A) and LLC-PK1 (B) cells were pretreated with the highest concentration of chloroquine, NH_4Cl, chlorpromazine, nystatin, EIPA, and wortmannin used in IPI-2I cells without resulting in obvious cytotoxic effects for 1 h at 37°C, respectively. Then, the cells were infected with PDCoV (MOI of 5) at 4°C for 1 h and then shifted to 37°C for 1 h (entry step). Cells were lysed to determine viral RNA copy numbers by RT-qPCR. The presented results represent the means and standard deviations of data from three independent experiments. **, $P < 0.01$.

Indirect immunofluorescence assay. The IFA was performed as described previously (63). Briefly, cells seeded onto coverslips in 24-well plates were treated according to various experiments and then harvested, fixed with 4% paraformaldehyde, and permeated with methanol. Treated cells were blocked with 5% bovine serum albumin, incubated separately with primary antibodies, treated with the secondary antibodies, including Alexa Fluor 488-conjugated donkey anti-mouse IgG and Alexa Fluor 594-conjugated donkey anti-rabbit IgG (Jackson ImmunoResearch, PA, USA), and stained with DAPI (4′,6-

TABLE 1 Primers used for the construction of plasmids and real-time RT-PCR assay

Primer	Nucleotide sequence
Dynamin-2-F	5-GATAAGGAATTCGAGCTCATCGATATGGGCA-3
Dynamin-2-R	5-GCAGAGGGAAAAAGATCTGCTAGCCTAGTCG-3
Caveolin-1-F	5-ATAATCGATATGTCGGGGGGCAAATACGTAG-3
Caveolin-1-R	5-GCGCTCGAGTTATATTTCTTTCTGCATGTTGATGC-3
Caveolin-1^{KSF}-F	5-GTGATCGATATGAAGAGTTTCCTGATTGAGATTC-3
Caveolin-1^{DGI}-F	5-TTGATCGATATGGATGGCATCTGGAAGGCCAGCTT-3
Rab5-F	5-GATGGTACCATGGCTAATCGAGGAGCAACAAGAC-3
Rab5-R	5-GGAAGATCTTTAGTTACTACAACACTGACTCCTG-3
Rab7-F	5-GATGGTACCATGACCTCTAGGAAGAAAGTGTTGC-3
Rab7-R	5-GGAAGATCTTCAGCAACTGCAGCTTTCTGCCGAG-3
Rab11-F	5-GATGGTACCATGGGCACCCGCGACGACGAGTACG-3
Rab11-R	5-GGAAGATCTTTAGATGTTCTGACAGCACTGCACC-3
qEPS15-F	5-ACCATGATGGGATGCTTGACA-3
qEPS15-R	5-GGACACAACCCACGTTTTCC-3
qCHC-F	5-ACAAAGGTGGATAAATTAGACGC-3
qCHC-R	5-CCCATAGGGTGGTGCAGTAT-3
qCaveolin 1-F	5-TACGTAGACTCAGAGGGACATC-3
qCaveolin 1-R	5-GTGTGCGCGTCATACACTTG-3
qDynamin-F	5-TCCCCAACCAGGTGATCCG-3
qDynamin-R	5-AGCCCTTTTCCACATCACGG-3
qRab5-F	5-GTCGATTTCCAGGAAGCACA-3
qRab5-R	5-GCGTGGGTTCAGTAAGGTCTA-3
qRab7-F	5-ATCCTGGGAGATTCTGGAGTTG-3
qRab7-R	5-GTAGAAGGCCACGCCAAGAG-3
qRab11-F	5-ATTTGCGTCATCTCAGGGCA-3
qRab11-R	5-ACAATGCGGTATATCTCTGTCA-3
qPDCoV-nsp16-F	5-GCCCTCGGTGGTTCTATCTT-3
qPDCoV-nsp16-R	5-TCCTTAGCTTGCCCCAAATA-3
qVSV-N-F	5-ACGGCGTACTTCCAGATGG-3
qVSV-N-R	5-CTCGGTTCAAGATCCAGGT-3
qSeV-HN-F	5-AAAATTACATGGCTAGGAGGGAAAC-3
qSeV-HN-R	5-GTGATTGGAATGGTTGTGACTCTTA-3
qGAPDH-F	5-ACATGGCCTCCAAGGAGTAAGA-3
qGAPDH-R	5-GATCGAGTTGGGGCTGTGACT-3

diamidino-2-phenylindole) for 15 min at room temperature. Fluorescent images were visualized using a confocal laser scanning microscope (Fluoview ver.3.1; Olympus, Japan) after three washes with phosphate-buffered saline (PBS).

Western blot analysis. The cells were washed with PBS and then lysed in 0.1 ml of lysis buffer (50 mM Tris-HCl, 150 mM NaCl, 1% NP-40, 10% glycerin, 0.1% SDS, and 2 mM Na_2EDTA, pH 7.4) for 30 min at 4°C. The lysates were clarified by centrifugation at 13,000 $\times$ *g* for 10 min. Supernatants from the lysates were separated by 12% SDS-PAGE and transferred to a polyvinylidene difluoride membrane (Millipore, Darmstadt, Germany). The membranes containing proteins were blocked with 5% nonfat milk in PBS with 0.1% polysorbate 20, treated with the indicated primary antibodies, and incubated with horseradish peroxidase-conjugated secondary antibodies (Beyotime). Finally, the membrane was visualized via enhanced chemiluminescence reagents (Bio-Rad, Hercules, CA, USA).

Statistical analysis. Statistical differences were determined using one-way analysis of variance or Student's *t* test using GraphPad Prism 5.0 software (GraphPad Software, CA, USA). For all experiments, *P* values of <0.05 were considered statistically significant.

TABLE 2 Sequence of siRNA used to abolish indicated protein expression

siRNA	Sequence
siCHC	5-UGACAAAGGUGGAUAAAUU-3
siCav1	5-CACACAGUUUCGAUGGCAUCUTT-3
siEPS15	5-GCUAGAUACCCUUAACAAUTT-3
sidynamin	5-CCUGCAGAAGACUCUGAAUTT-3
siRab5	5-GCAAGCCAGUCCUAACAUUTT-3
siRab7	5-GCUCUACAAUGAAUUCCCUTT-3
siRab11	5-GCAAAUGUCAGACAGACGUTT-3
siCtrl (negative control)	5-UUCUCCGAACGUGUCACGUTT-3

ACKNOWLEDGMENTS

We thank Zhigao Bu and Stephen S. G. Ferguson for providing agents.

This work was supported by the National Natural Science Foundation of China (31730095, U1704231, 31902247, and 32072846) and the China Postdoctoral Science Foundation (2019T120670 and 2018M640717).

REFERENCES

1. Yang YL, Liang QZ, Xu SY, Mazing E, Xu GH, Peng L, Qin P, Wang B, Huang YW. 2019. Characterization of a novel bat-HKU2-like swine enteric alphacoronavirus (SeACoV) infection in cultured cells and development of a SeACoV infectious clone. Virology 536:110–118. https://doi.org/10.1016/j.virol.2019.08.006.
2. Dong N, Fang L, Yang H, Liu H, Du T, Fang P, Wang D, Chen H, Xiao S. 2016. Isolation, genomic characterization, and pathogenicity of a Chinese porcine deltacoronavirus strain CHN-HN-2014. Vet Microbiol 196:98–106. https://doi.org/10.1016/j.vetmic.2016.10.022.
3. Liang Q, Zhang H, Li B, Ding Q, Wang Y, Gao W, Guo D, Wei Z, Hu H. 2019. Susceptibility of chickens to porcine deltacoronavirus infection. Viruses 11:573. https://doi.org/10.3390/v11060573.
4. Hu H, Jung K, Vlasova AN, Saif LJ. 2016. Experimental infection of gnotobiotic pigs with the cell-culture-adapted porcine deltacoronavirus strain OH-FD22. Arch Virol 161:3421–3434. https://doi.org/10.1007/s00705-016-3056-8.
5. Zhang J, Chen J, Liu Y, Da S, Shi H, Zhang X, Liu J, Cao L, Zhu X, Wang X, Ji Z, Feng L. 2020. Pathogenicity of porcine deltacoronavirus (PDCoV) strain NH and immunization of pregnant sows with an inactivated PDCoV vaccine protects 5-day-old neonatal piglets from virulent challenge. Transbound Emerg Dis 67:572–583. https://doi.org/10.1111/tbed.13369.
6. Chen Q, Gauger P, Stafne M, Thomas J, Arruda P, Burrough E, Madson D, Brodie J, Magstadt D, Derscheid R, Welch M, Zhang J. 2015. Pathogenicity and pathogenesis of a United States porcine deltacoronavirus cell culture isolate in 5-day-old neonatal piglets. Virology 482:51–59. https://doi.org/10.1016/j.virol.2015.03.024.
7. Woo PC, Lau SK, Lam CS, Lau CC, Tsang AK, Lau JH, Bai R, Teng JL, Tsang CC, Wang M, Zheng BJ, Chan KH, Yuen KY. 2012. Discovery of seven novel mammalian and avian coronaviruses in the genus Deltacoronavirus supports bat coronaviruses as the gene source of Alphacoronavirus and Betacoronavirus and avian coronaviruses as the gene source of Gammacoronavirus and Deltacoronavirus. J Virol 86:3995–4008. https://doi.org/10.1128/JVI.06540-11.
8. Li G, Chen Q, Harmon KM, Yoon KJ, Schwartz KJ, Hoogland MJ, Gauger PC, Main RG, Zhang J. 2014. Full-length genome sequence of porcine Deltacoronavirus strain USA/IA/2014/8734. Genome Announc 2:e00278-14. https://doi.org/10.1128/genomeA.00278-14.
9. Lorsirigool A, Saeng-Chuto K, Madapong A, Temeeyasen G, Tripipat T, Kaewprommal P, Tantituvanont A, Piriyapongsa J, Nilubol D. 2017. The genetic diversity and complete genome analysis of two novel porcine deltacoronavirus isolates in Thailand in 2015. Virus Genes 53:240–248. https://doi.org/10.1007/s11262-016-1413-z.
10. Jang G, Lee KK, Kim SH, Lee C. 2017. Prevalence, complete genome sequencing and phylogenetic analysis of porcine deltacoronavirus in South Korea, 2014–2016. Transbound Emerg Dis 64:1364–1370. https://doi.org/10.1111/tbed.12690.
11. Saeng-Chuto K, Lorsirigool A, Temeeyasen G, Vui DT, Stott CJ, Madapong A, Tripipat T, Wegner M, Intrakamhaeng M, Chongcharoen W, Tantituvanont A, Kaewprommal P, Piriyapongsa J, Nilubol D. 2017. Different lineage of porcine deltacoronavirus in Thailand, Vietnam and Lao PDR in 2015. Transbound Emerg Dis 64:3–10. https://doi.org/10.1111/tbed.12585.
12. Dong N, Fang L, Zeng S, Sun Q, Chen H, Xiao S. 2015. Porcine Deltacoronavirus in mainland China. Emerg Infect Dis 21:2254–2255. https://doi.org/10.3201/eid2112.150283.
13. Xu Z, Zhong H, Zhou Q, Du Y, Chen L, Zhang Y, Xue C, Cao Y. 2018. A highly pathogenic strain of porcine Deltacoronavirus caused watery diarrhea in newborn piglets. Virol Sin 33:131–141. https://doi.org/10.1007/s12250-018-0003-8.
14. Boley PA, Alhamo MA, Lossie G, Yadav KK, Vasquez-Lee M, Saif LJ, Kenney SP. 2020. Porcine Deltacoronavirus infection and transmission in poultry, United States. Emerg Infect Dis 26:255–265. https://doi.org/10.3201/eid2602.190346.
15. Jung K, Hu H, Saif LJ. 2017. Calves are susceptible to infection with the newly emerged porcine deltacoronavirus, but not with the swine enteric alphacoronavirus, porcine epidemic diarrhea virus. Arch Virol 162:2357–2362. https://doi.org/10.1007/s00705-017-3351-z.
16. Lednicky JA, Tagliamonte MS, White SK, Elbadry MA, Alam MM, Stephenson CJ, Bonny TS, Loeb JC, Telisma T, Chavannes S, Ostrov DA, Mavian C, De Rochars VMB, Salemi M, Morris JG. 2021. Emergence of porcine delta-coronavirus pathogenic infections among children in Haiti through independent zoonoses and convergent evolution. medRxiv https://doi.org/10.1101/2021.03.19.21253391.
17. Li W, Hulswit RJG, Kenney SP, Widjaja I, Jung K, Alhamo MA, van Dieren B, van Kuppeveld FJM, Saif LJ, Bosch BJ. 2018. Broad receptor engagement of an emerging global coronavirus may potentiate its diverse cross-species transmissibility. Proc Natl Acad Sci U S A 115:E5135–E5143. https://doi.org/10.1073/pnas.1802879115.
18. Pelkmans L, Helenius A. 2003. Insider information: what viruses tell us about endocytosis. Curr Opin Cell Biol 15:414–422. https://doi.org/10.1016/s0955-0674(03)00081-4.
19. Sun X, Yau VK, Briggs BJ, Whittaker GR. 2005. Role of clathrin-mediated endocytosis during vesicular stomatitis virus entry into host cells. Virology 338:53–60. https://doi.org/10.1016/j.virol.2005.05.006.
20. Sanchez EG, Perez-Nunez D, Revilla Y. 2017. Mechanisms of entry and endosomal pathway of African swine fever virus. Vaccines (Basel) 5:42. https://doi.org/10.3390/vaccines5040042.
21. Piccinotti S, Whelan SP. 2016. Rabies internalizes into primary peripheral neurons via clathrin coated pits and requires fusion at the cell body. PLoS Pathog 12:e1005753. https://doi.org/10.1371/journal.ppat.1005753.
22. Krishnan MN, Sukumaran B, Pal U, Agaisse H, Murray JL, Hodge TW, Fikrig E. 2007. Rab 5 is required for the cellular entry of dengue and West Nile viruses. J Virol 81:4881–4885. https://doi.org/10.1128/JVI.02210-06.
23. Zhang YN, Liu YY, Xiao FC, Liu CC, Liang XD, Chen J, Zhou J, Baloch AS, Kan L, Zhou B, Qiu HJ. 2018. Rab5, Rab7, and Rab11 are required for caveola-dependent endocytosis of classical swine fever virus in porcine alveolar macrophages. J Virol 92:e00797-18. https://doi.org/10.1128/JVI.00797-18.
24. Elgner F, Hildt E, Bender D. 2018. Relevance of Rab proteins for the life cycle of hepatitis C virus. Front Cell Dev Biol 6:166. https://doi.org/10.3389/fcell.2018.00166.
25. Mercer J, Schelhaas M, Helenius A. 2010. Virus entry by endocytosis. Annu Rev Biochem 79:803–833. https://doi.org/10.1146/annurev-biochem-060208-104626.
26. Nomura R, Kiyota A, Suzaki E, Kataoka K, Ohe Y, Miyamoto K, Senda T, Fujimoto T. 2004. Human coronavirus 229E binds to CD13 in rafts and enters the cell through caveolae. J Virol 78:8701–8708. https://doi.org/10.1128/JVI.78.16.8701-8708.2004.
27. Werling D, Hope JC, Chaplin P, Collins RA, Taylor G, Howard CJ. 1999. Involvement of caveolae in the uptake of respiratory syncytial virus antigen by dendritic cells. J Leukoc Biol 66:50–58. https://doi.org/10.1002/jlb.66.1.50.
28. Han SC, Guo HC, Sun SQ, Jin Y, Wei YQ, Feng X, Yao XP, Cao SZ, Xiang Liu D, Liu XT. 2016. Productive entry of foot-and-mouth disease virus via macropinocytosis independent of phosphatidylinositol 3-kinase. Sci Rep 6:19294. https://doi.org/10.1038/srep19294.
29. Rossman JS, Leser GP, Lamb RA. 2012. Filamentous influenza virus enters cells via macropinocytosis. J Virol 86:10950–10960. https://doi.org/10.1128/JVI.05992-11.
30. Sanchez EG, Quintas A, Perez-Nunez D, Nogal M, Barroso S, Carrascosa AL, Revilla Y. 2012. African swine fever virus uses macropinocytosis to enter host cells. PLoS Pathog 8:e1002754. https://doi.org/10.1371/journal.ppat.1002754.
31. Nanbo A, Imai M, Watanabe S, Noda T, Takahashi K, Neumann G, Halfmann P, Kawaoka Y. 2010. Ebolavirus is internalized into host cells via macropinocytosis in a viral glycoprotein-dependent manner. PLoS Pathog 6:e1001121. https://doi.org/10.1371/journal.ppat.1001121.
32. Jeon JH, Lee C. 2018. Cholesterol is important for the entry process of porcine deltacoronavirus. Arch Virol 163:3119–3124. https://doi.org/10.1007/s00705-018-3967-7.

33. Zhang J, Chen J, Shi D, Shi H, Zhang X, Liu J, Cao L, Zhu X, Liu Y, Wang X, Ji Z, Feng L. 2019. Porcine deltacoronavirus enters cells via two pathways: a protease-mediated one at the cell surface and another facilitated by cathepsins in the endosome. J Biol Chem 294:9830–9843. https://doi.org/10.1074/jbc.RA119.007779.
34. Hernandez LD, Hoffman LR, Wolfsberg TG, White JM. 1996. Virus-cell and cell-cell fusion. Annu Rev Cell Dev Biol 12:627–661. https://doi.org/10.1146/annurev.cellbio.12.1.627.
35. Chejanovsky N, Henis YI, Loyter A. 1986. Fusion of fluorescently labeled Sendai virus envelopes with living cultured cells as monitored by fluorescence dequenching. Exp Cell Res 164:353–365. https://doi.org/10.1016/0014-4827(86)90034-0.
36. Liu CC, Zhang YN, Li ZY, Hou JX, Zhou J, Kan L, Zhou B, Chen PY. 2017. Rab5 and Rab11 are required for clathrin-dependent endocytosis of Japanese encephalitis virus in BHK-21 cells. J Virol 91:e01113-17. https://doi.org/10.1128/JVI.01113-17.
37. Benmerah A, Bayrou M, Cerf-Bensussan N, Dautry-Varsat A. 1999. Inhibition of clathrin-coated pit assembly by an Eps15 mutant. J Cell Sci 112:1303–1311. https://doi.org/10.1242/jcs.112.9.1303.
38. Norkin LC, Kuksin D. 2005. The caveolae-mediated sv40 entry pathway bypasses the Golgi complex en route to the endoplasmic reticulum. Virol J 2:38. https://doi.org/10.1186/1743-422X-2-38.
39. Orth JD, Krueger EW, Cao H, McNiven MA. 2002. The large GTPase dynamin regulates actin comet formation and movement in living cells. Proc Natl Acad Sci U S A 99:167–172. https://doi.org/10.1073/pnas.012607899.
40. Koivusalo M, Welch C, Hayashi H, Scott CC, Kim M, Alexander T, Touret N, Hahn KM, Grinstein S. 2010. Amiloride inhibits macropinocytosis by lowering submembranous pH and preventing Rac1 and Cdc42 signaling. J Cell Biol 188:547–563. https://doi.org/10.1083/jcb.200908086.
41. Li Q, Fischer E, Cohen JI. 2016. Cell surface THY-1 contributes to human cytomegalovirus entry via a macropinocytosis-like process. J Virol 90:9766–9781. https://doi.org/10.1128/JVI.01092-16.
42. Yang YL, Meng F, Qin P, Herrler G, Huang YW, Tang YD. 2020. Trypsin promotes porcine deltacoronavirus mediating cell-to-cell fusion in a cell type-dependent manner. Emerg Microbes Infect 9:457–468. https://doi.org/10.1080/22221751.2020.1730245.
43. Li Z, Zhao K, Lan Y, Lv X, Hu S, Guan J, Lu H, Zhang J, Shi J, Yang Y, Song D, Gao F, He W. 2017. Porcine hemagglutinating encephalomyelitis virus enters neuro-2a cells via clathrin-mediated endocytosis in a Rab5-, cholesterol-, and pH-dependent manner. J Virol 91:e01083-17. https://doi.org/10.1128/JVI.01083-17.
44. Shi BJ, Liu CC, Zhou J, Wang SQ, Gao ZC, Zhang XM, Zhou B, Chen PY. 2016. Entry of Classical swine fever virus into PK-15 cells via a pH-, dynamin-, and cholesterol-dependent, clathrin-mediated endocytic pathway that requires Rab5 and Rab7. J Virol 90:9194–9208. https://doi.org/10.1128/JVI.00688-16.
45. Wang B, Liu Y, Ji CM, Yang YL, Liang QZ, Zhao P, Xu LD, Lei XM, Luo WT, Qin P, Zhou J, Huang YW. 2018. Porcine Deltacoronavirus engages the transmissible gastroenteritis virus functional receptor porcine aminopeptidase N for infectious cellular entry. J Virol 92:e00318-18. https://doi.org/10.1128/JVI.00318-18.
46. Zhu X, Liu S, Wang X, Luo Z, Shi Y, Wang D, Peng G, Chen H, Fang L, Xiao S. 2018. Contribution of porcine aminopeptidase N to porcine deltacoronavirus infection. Emerg Microbes Infect 7:65. https://doi.org/10.1038/s41426-018-0068-3.
47. Stoian A, Rowland RRR, Petrovan V, Sheahan M, Samuel MS, Whitworth KM, Wells KD, Zhang J, Beaton B, Cigan M, Prather RS. 2020. The use of cells from ANPEP knockout pigs to evaluate the role of aminopeptidase N (APN) as a receptor for porcine deltacoronavirus (PDCoV). Virology 541:136–140. https://doi.org/10.1016/j.virol.2019.12.007.
48. Xu K, Zhou Y, Mu Y, Liu Z, Hou S, Xiong Y, Fang L, Ge C, Wei Y, Zhang X, Xu C, Che J, Fan Z, Xiang G, Guo J, Shang H, Li H, Xiao S, Li J, Li K. 2020. CD163 and pAPN double-knockout pigs are resistant to PRRSV and TGEV and exhibit decreased susceptibility to PDCoV while maintaining normal production performance. Elife 9:e57132. https://doi.org/10.7554/eLife.57132.
49. Wang H, Yang P, Liu K, Guo F, Zhang Y, Zhang G, Jiang C. 2008. SARS coronavirus entry into host cells through a novel clathrin- and caveolae-independent endocytic pathway. Cell Res 18:290–301. https://doi.org/10.1038/cr.2008.15.
50. Nabi IR, Le PU. 2003. Caveolae/raft-dependent endocytosis. J Cell Biol 161:673–677. https://doi.org/10.1083/jcb.200302028.
51. Yang S, He M, Liu X, Li X, Fan B, Zhao S. 2013. Japanese encephalitis virus infects porcine kidney epithelial PK15 cells via clathrin- and cholesterol-dependent endocytosis. Virol J 10:258. https://doi.org/10.1186/1743-422X-10-258.
52. Zhu YZ, Xu QQ, Wu DG, Ren H, Zhao P, Lao WG, Wang Y, Tao QY, Qian XJ, Wei YH, Cao MM, Qi ZT. 2012. Japanese encephalitis virus enters rat neuroblastoma cells via a pH-dependent, dynamin and caveola-mediated endocytosis pathway. J Virol 86:13407–13422. https://doi.org/10.1128/JVI.00903-12.
53. Zhao R, Shi Q, Han Z, Fan Z, Ai H, Chen L, Li L, Liu T, Sun J, Liu S. 2021. Newcastle disease virus entry into chicken macrophages via a pH-dependent, dynamin and caveola-mediated endocytic pathway that requires Rab5. J Virol 95:e0228820. https://doi.org/10.1128/JVI.02288-20.
54. Inoue Y, Tanaka N, Tanaka Y, Inoue S, Morita K, Zhuang M, Hattori T, Sugamura K. 2007. Clathrin-dependent entry of severe acute respiratory syndrome coronavirus into target cells expressing ACE2 with the cytoplasmic tail deleted. J Virol 81:8722–8729. https://doi.org/10.1128/JVI.00253-07.
55. Amyere M, Payrastre B, Krause U, Van Der Smissen P, Veithen A, Courtoy PJ. 2000. Constitutive macropinocytosis in oncogene-transformed fibroblasts depends on sequential permanent activation of phosphoinositide 3-kinase and phospholipase C. Mol Biol Cell 11:3453–3467. https://doi.org/10.1091/mbc.11.10.3453.
56. Bai D, Fang L, Xia S, Ke W, Wang J, Wu X, Fang P, Xiao S. 2020. Porcine deltacoronavirus (PDCoV) modulates calcium influx to favor viral replication. Virology 539:38–48. https://doi.org/10.1016/j.virol.2019.10.011.
57. Murray JL, Mavrakis M, McDonald NJ, Yilla M, Sheng J, Bellini WJ, Zhao L, Le Doux JM, Shaw MW, Luo CC, Lippincott-Schwartz J, Sanchez A, Rubin DH, Hodge TW. 2005. Rab9 GTPase is required for replication of human immunodeficiency virus type 1, filoviruses, and measles virus. J Virol 79:11742–11751. https://doi.org/10.1128/JVI.79.18.11742-11751.2005.
58. Wei X, She G, Wu T, Xue C, Cao Y. 2020. PEDV enters cells through clathrin-, caveolae-, and lipid raft-mediated endocytosis and traffics via the endo-/lysosome pathway. Vet Res 51:10. https://doi.org/10.1186/s13567-020-0739-7.
59. Burkard C, Verheije MH, Wicht O, van Kasteren SI, van Kuppeveld FJ, Haagmans BL, Pelkmans L, Rottier PJ, Bosch BJ, de Haan CA. 2014. Coronavirus cell entry occurs through the endo-/lysosomal pathway in a proteolysis-dependent manner. PLoS Pathog 10:e1004502. https://doi.org/10.1371/journal.ppat.1004502.
60. Wang H, Yuan X, Sun Y, Mao X, Meng C, Tan L, Song C, Qiu X, Ding C, Liao Y. 2019. Infectious bronchitis virus entry mainly depends on clathrin mediated endocytosis and requires classical endosomal/lysosomal system. Virology 528:118–136. https://doi.org/10.1016/j.virol.2018.12.012.
61. Luo J, Fang L, Dong N, Fang P, Ding Z, Wang D, Chen H, Xiao S. 2016. Porcine deltacoronavirus (PDCoV) infection suppresses RIG-I-mediated interferon-beta production. Virology 495:10–17. https://doi.org/10.1016/j.virol.2016.04.025.
62. Roy S, Luetterforst R, Harding A, Apolloni A, Etheridge M, Stang E, Rolls B, Hancock JF, Parton RG. 1999. Dominant-negative caveolin inhibits H-Ras function by disrupting cholesterol-rich plasma membrane domains. Nat Cell Biol 1:98–105. https://doi.org/10.1038/10067.
63. Fang P, Fang L, Ren J, Hong Y, Liu X, Zhao Y, Wang D, Peng G, Xiao S. 2018. Porcine Deltacoronavirus accessory protein NS6 antagonizes interferon beta production by interfering with the binding of RIG-I/MDA5 to double-stranded RNA. J Virol 92:e00712-18. https://doi.org/10.1128/JVI.00712-18.